Title

Tracking Rh Atoms in Zeolite HY: First Steps of Metal Cluster Formation and Influence of Metal Nuclearity on Catalysis of Ethylene Hydrogenation and Ethylene Dimerization

Journal

The Journal of Physical Chemistry Letters, 7(13)

ISSN

1948-7185

Authors

Yang, Dong
Xu, Pinghong
Browning, Nigel D
et al.

Publication Date

2016-07-07

DOI

10.1021/acs.jpclett.6b01153

Peer reviewed

Tracking Rh Atoms in Zeolite HY: First Steps of Metal Cluster Formation and Influence of Metal Nuclearity on Catalysis of Ethylene Hydrogenation and Ethylene Dimerization

Dong Yang,[a]† *Pinghong Xu,*[a]† *Nigel D. Browning,*[b] *Bruce C. Gates*[a,*]

[a] Department of Chemical Engineering, University of California, Davis, CA 95616, United States

[b] Physical and Computational Sciences, Pacific Northwest National Laboratory, 902 Battelle Blvd, Richland, WA 99352, United States

AUTHOR INFORMATION

Corresponding Author

* Bruce C. Gates, Email: bcgates@ucdavis.edu

ABSTRACT. The initial steps of rhodium cluster formation from zeolite-supported mononuclear $Rh(C_2H_4)_2$ complexes in H_2 at 373 K and 1 bar were investigated by infrared and extended X-ray absorption fine structure spectroscopies and scanning transmission electron microscopy (STEM). The data show that ethylene ligands on the rhodium react with H_2 to give supported rhodium hydrides and trigger the formation of rhodium clusters. STEM provided the first images of the smallest rhodium clusters (Rh_2) and their further conversion into larger clusters. The samples were investigated in a plug-flow reactor as catalysts for the conversion of ethylene + H_2 in a molar ratio of 4:1 at 1 bar and 298 K, with the results showing how the changes in catalyst structure affect the activity and selectivity; the rhodium clusters are more active for hydrogenation of ethylene than the single-site complexes, which are more selective for dimerization of ethylene to give butenes.

TOC GRAPHICS

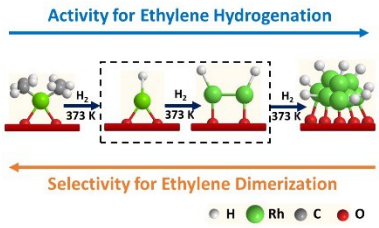

KEYWORDS Zeolite HY, single-site catalyst, surface pair sites, rhodium cluster formation, rhodium, STEM image.

Single-site catalysts comprising isolated metal ions on solid surfaces are drawing increasing attention because they evidently offer new, tailorable catalytic properties[1-6] and because the metals, if they are heavy and present on supports that consist of light elements, can sometimes be imaged by aberration-corrected scanning transmission electron microscopy (STEM).[7-11] A step toward increasing complexity of such catalysts involves the synthesis of pairs of metal centers on supports, and these offer prospects of new properties associated with the neighboring metal centers. There are still only a small number of catalysts in this class.[12-16]

We now report supported metal catalysts consisting initially of isolated Rh centers on a support, zeolite HY, and its transformation in the presence of H_2 to form rhodium pair sites and then larger rhodium clusters. The data reported here indicate how the transformation of the rhodium species leads to changes in the catalytic properties of the rhodium, and they thus lay a foundation for how to tailor supported rhodium catalysts. The supported species were characterized by infrared (IR) and X-ray absorption spectra complemented by STEM images that provide the first direct evidence of the first steps of rhodium cluster formation. HY zeolite was chosen as the catalyst support because it consists of light atoms for contrast with the Rh atoms in imaging and because it is crystalline, facilitating the formation of uniform rhodium species initially on its surface. Rhodium was chosen as the catalytic species because of its rich catalytic chemistry in forms ranging from isolated cationic complexes[17-25] to small clusters[26-29] to larger metallic particles.[30-33] The catalytic properties of the supported rhodium species were probed with ethylene hydrogenation and ethylene dimerization as test reactions, because these reactions take place under mild conditions that minimize changes in structure of the rhodium species[12, 34-35] and because ethylene and H_2 form ligands on the rhodium that are identifiable by IR spectroscopy.

The results presented here demonstrate that H_2 dissociation takes place on the supported rhodium complexes, leading to the formation of rhodium hydride and the removal of ethylene ligands to trigger rhodium cluster formation. STEM images confirm that the initial step of metal cluster formation is the formation of dirhodium species. Moreover, our data show how the nuclearity and ligand environment change during the earliest stages of cluster formation and thereby change the catalytic activity and selectivity in the conversion of ethylene with H_2.

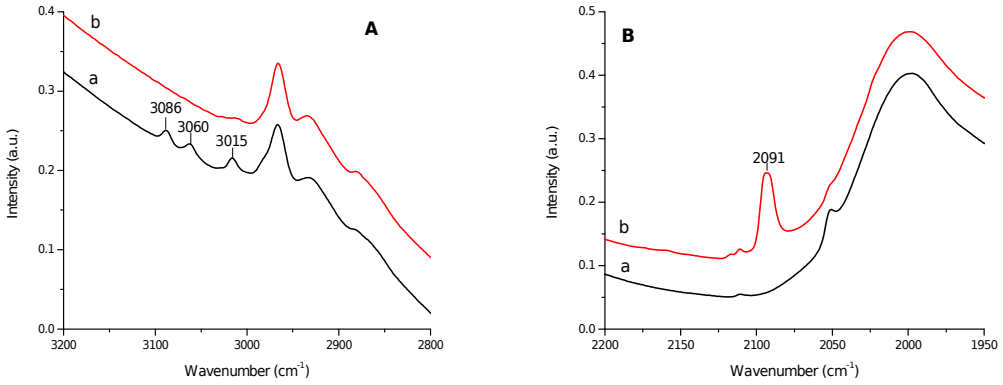

Figure 1. IR spectra in (A) the ν_{CH} region and (B) the ν_H/ν_{CO} region characterizing the HY zeolite-supported $Rh(C_2H_4)_2$ in (a) flowing helium and (b) after the sample had been in contact with flowing H_2 in helium for 4 min at 373 K and 1 bar.

Structurally well-defined HY zeolite-supported $Rh(C_2H_4)_2$ complexes were synthesized as before[18] by reaction of $Rh(C_2H_4)_2(acac)$ (acac is acetylacetonate) with dealuminated HY zeolite (Si/Al atomic ratio = 30). IR and extended X-ray absorption fine structure (EXAFS) spectra characterizing the supported species confirm the identity of the rhodium diethylene complex, with the EXAFS data showing that each Rh atom was anchored to the support by two Rh–O bonds. The IR spectra show bands in the C–H stretching region, between 3000 and 3100 cm^{-1}

(Figure 1), assigned to π-bonded ethylene ligands on the basis of a comparison of the spectrum with spectra of reference compounds such as $K[PtCl_3(C_2H_4)]$ and that of ethylene adsorbed on supported platinum particles, as well as DFT calculations.[19] The EXAFS data show that each Rh atom was bonded, on average, to two ethylene ligands, evidenced by the Rh–C coordination number of nearly 4 (Table 1). These results are as expected on the basis of reported results.[18-19]

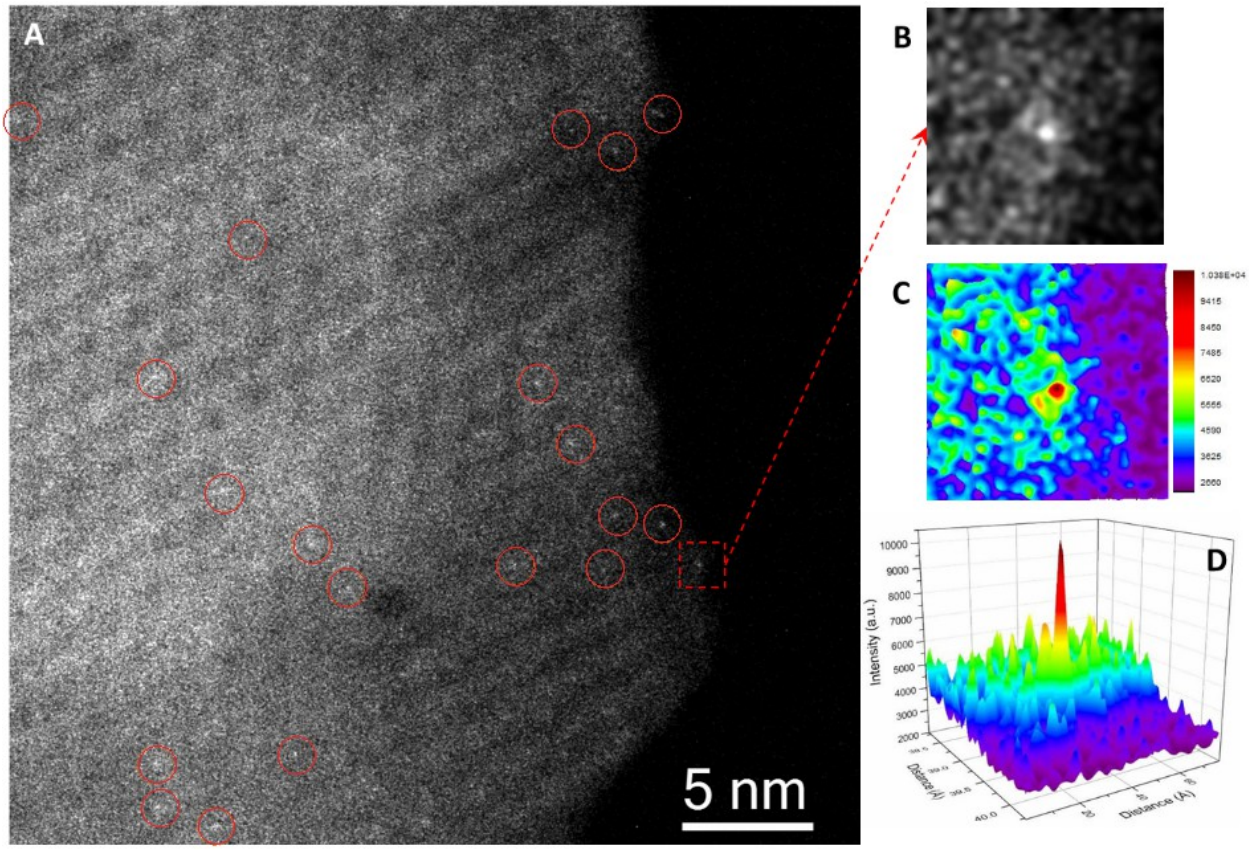

Figure 2. A, aberration-corrected HAADF-STEM image characterizing $[Rh(C_2H_4)_2]^+$ complexes on zeolite HY, indicating isolated Rh sites. Bright features encircled are examples of individual Rh atoms. B, magnified view of the dashed-square area in A containing one Rh atom, with intensity surface plot shown in C and 3-dimensional intensity surface plot shown in D.

Table 1. EXAFS structure parameters representing $Rh(C_2H_4)_2$ supported on dealuminated HY zeolite after various treatments.[a]

Treatment conditions	Shell	*N*	*R* (Å)	$10^3 \times \Delta\sigma^2$ (Å^2)	ΔE_0 (eV)	Ref
None	Rh–Rh	[b]	[b]	[b]	[b]	This work
	$Rh–O_s$	2.0	2.08	6.0	3.4	
	Rh–C	3.9	2.05	1.9	4.8	
	Rh–Al	1.2	3.01	4.8	-1.3	
	$Rh–O_{long}$	2.2	3.35	6.8	-7.6	
H_2 in flowing helium, 1 bar, 373 K, 4 min	Rh–Rh	0.18	2.62	6.5	-0.3	This work
	$Rh–O_s$	1.9	2.07	6.9	-4.1	
	Rh–C	[b]	[b]	[b]	[b]	
	Rh–Al	0.9	2.97	1.5	2.4	
	$Rh–O_{long}$	0.5	3.51	0.8	-8.0	
H_2 in flowing helium, 1 bar, 373 K, 60 min	Rh–Rh	4.4	2.67	9.2	4.0	[36]
	$Rh–O_s$	0.6	2.18	1.6	-7.2	
	Rh–C	[b]	[b]	[b]	[b]	

[a]Notation: O_s, surface oxygen on top of Al sites; C, ethylene carbon; *N*, coordination number; *R*, distance between absorber and backscatterer atoms; $\Delta\sigma^2$, disorder term; ΔE_0, inner potential correction. Estimated EXAFS error bounds: *N*, ±20%; *R*, ±0.02 Å; $\Delta\sigma^2$, ±20%; ΔE_0, ±20% (errors characterizing the Rh−Al contribution are greater than these). [b]Contribution not detectable.

STEM was used to image the Rh atoms in the initially prepared sample, with the results (Figure 2) providing evidence of the site-isolated Rh atoms, consistent with the IR and EXAFS data. This is the first image of isolated zeolite-supported Rh atoms. *Z*-contrast imaging is well-suited to characterization of our samples because of the high atomic number difference between the Rh atoms (*Z* number 45) and the atoms comprising the support (*Z* numbers for Si, Al, and O 14, 13, and 8, respectively). To obtain the image of Figure 2, a high-dose approach (~10^5–10^8 e^-/A^2) was applied for a high signal-to-noise ratio, resulting in the lack of need for post-image simulation, in contrast earlier work with low-dose imaging.[8] The bright features highlighted in Figure 2 are individual Rh atoms. The image gives no evidence of rhodium clusters or particles, in agreement with the EXAFS data, which give no evidence of Rh–Rh contributions (Table 1).

The stability of the mononuclear supported rhodium present initially in the sample was demonstrated as the temperature was ramped from 298 to 373 K with the sample in flowing helium with no detectable change in the IR (Supporting Information, SI, Figure S1) and EXAFS spectra (SI, Table S1).

When the composition of the gas flowing over the catalyst sample at 373 K was switched from helium to H_2, the initially π-bonded ethylene ligands in the supported $Rh(C_2H_4)_2$ complexes were immediately replaced by hydride, as shown by the disappearance of IR bands characteristic of C_2H_4 ligands, at 3086, 3060, and 3015 cm^{-1}, and a concomitant growth of a Rh–H band, at 2091 cm^{-1} [19, 35] (Figure 1). Exposure of the sample to D_2 instead of H_2 correspondingly led to the formation of Rh–D species, characterized by an IR band at 1486 cm^{-1} (with the ratio of frequencies of Rh–D to Rh–H species consistent with the harmonic approximation).[19, 35] Furthermore, the mass spectra of the effluent gas gave evidence of ethane, showing that ethylene had undergone hydrogenation with the reactant H_2.

In agreement with the IR data, EXAFS data characterizing the supported $Rh(C_2H_4)_2$ species show the disappearance of the Rh–C contribution after 4 min of contact of the sample with H_2 at 373 K, accompanied by the appearance of a small contribution identified as Rh–Rh at a distance of 2.62 Å, which indicates the very beginning of formation of rhodium clusters. Simultaneously, the coordination numbers characterizing the $Rh–O_s$ (the subscript refers to surface) and Rh–Al contributions decreased slightly, from 2.0 and 1.2 to 1.9 and 0.9, respectively, after the treatment. The EXAFS results indicate that each rhodium hydride complex was still bonded to approximately two support oxygen atoms, on average.

Figure 3 is a STEM image of the catalyst after treatment in flowing 50% H_2 in helium at 373 K and 1 bar for 4 min, indicating the presence of supported rhodium dimers along with Rh single atoms. The two rhodium atoms in the dimer match each other in intensity (Figure 3D). The majority of Rh atoms were present as these mononuclear species, with only approximately 24% of them present in the pair sites (12 of 50). The images gave no evidence of groupings of three or more Rh atoms. The average coordination number determined by STEM is approximately 0.12, which is close to the EXAFS value charactering the Rh–Rh coordination number (0.18).

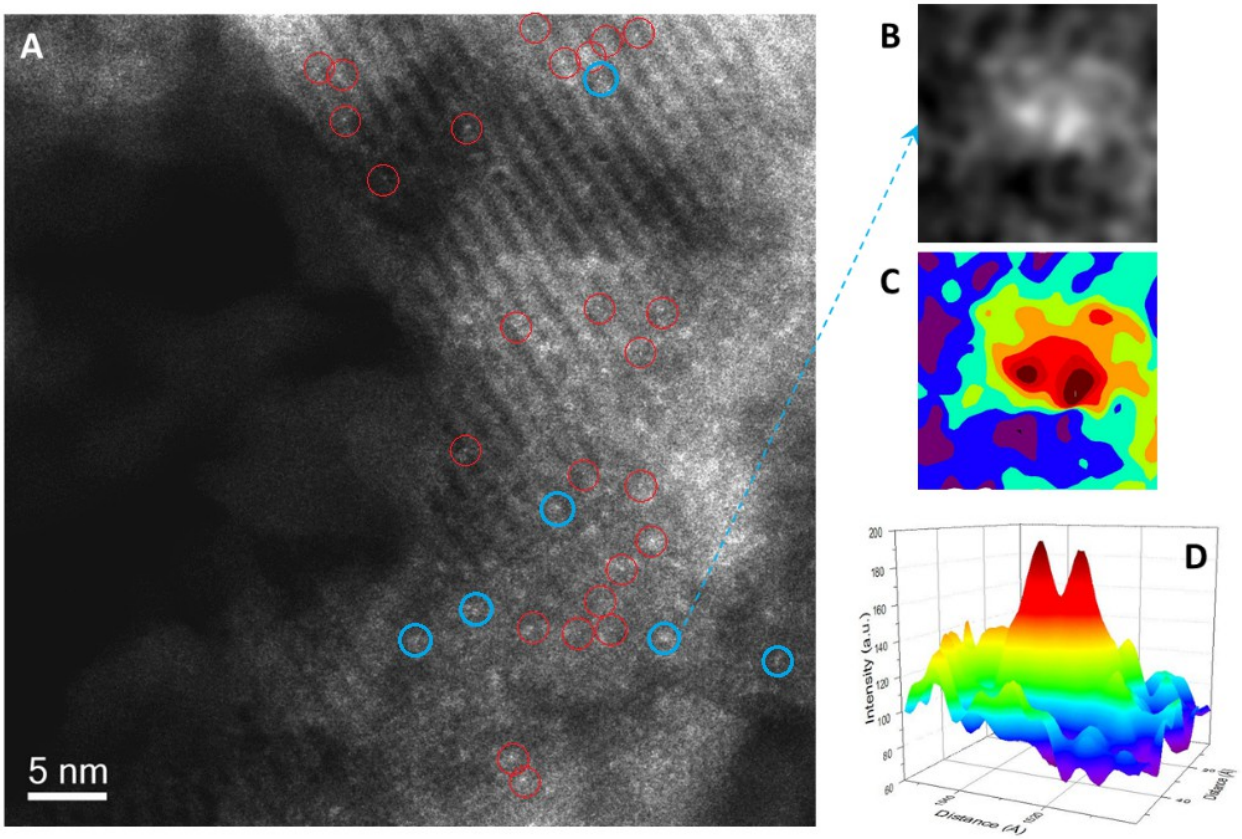

Figure 3. Aberration-corrected HAADF-STEM images characterizing $[Rh(C_2H_4)_2]^+$ complexes in zeolite Y, after treatment in flowing H_2/He at 373 K and 1 bar for 4 min, indicating the presence of supported Rh dimers (encircled in blue) along with single isolated Rh atoms (encircled in red). Bright features encircled are examples of individual Rh atoms or dimers. (B) A magnified view of the encircled area in (A) containing one Rh pair site, with intensity surface plot shown in (C) and 3-dimensional intensity surface plot shown in (D).

These results show that rhodium dimer formation is the first step of formation of larger rhodium clusters on the zeolite surface. The process is trigged by the removal of ethylene ligands and the activation of hydrogen and formation of rhodium hydride species.

To track the further metal cluster formation, we treated the sample in a flowing 50% H_2 in helium at 1 bar and 373 K for 60 min. The EXAFS data of Table 1 show that the Rh–Rh coordination number increased to 4.4 as a result of the reaction with H_2, indicating clusters with an average diameter of about 5–6 Å (this average size corresponds to a metal dispersion of nearly 100% and indicates that each cluster incorporates, on average, approximately nine atoms if spherical clusters are assumed[37-38]). The growth of the rhodium clusters was accompanied by a decrease in the EXAFS-determined coordination number characterizing the Rh–O_s contribution (from 1.9 to 0.6), demonstrating the unlinking of the rhodium complex from the support as the Rh atoms migrated and aggregated.

The STEM images exemplified by Figure 4 confirm the presence of rhodium clusters larger than dimers, and analysis of the images determined an average rhodium cluster diameter of 0.55 ± 0.10 nm, which agrees well with the diameter estimated on the basis of the EXAFS data. The images show that the rhodium clusters were mostly smaller than 8 Å in diameter. We emphasize that site-isolated single Rh atoms were also observed in small numbers in this sample along with the clusters, indicating that not all of the rhodium had been converted into clusters during the treatment in H_2.

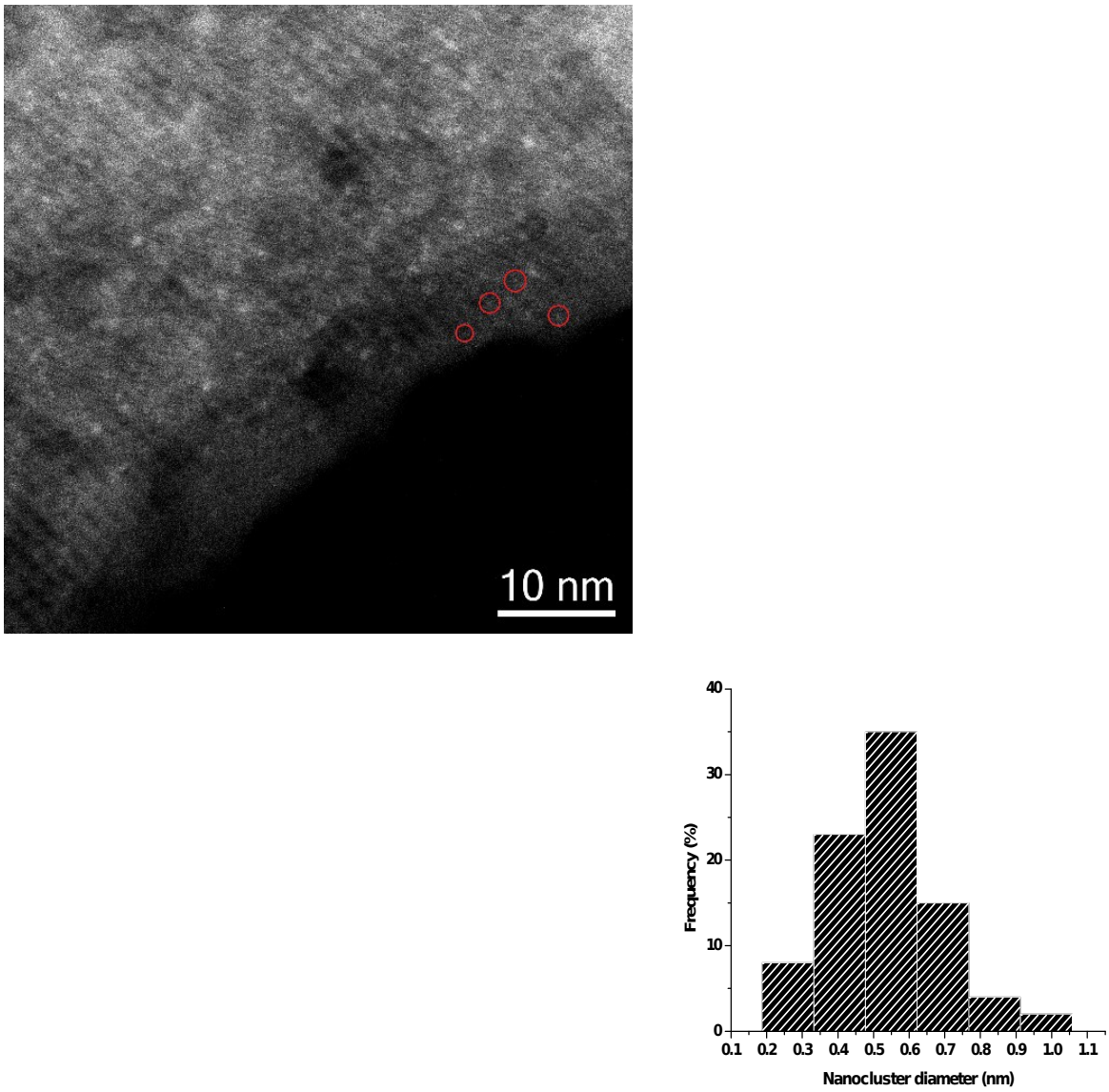

Figure 4. Aberration-corrected HAADF-STEM image characterizing rhodium clusters in zeolite HY, after treatment of the initially prepared sample in flowing H_2 at 1 bar and 373 K for 1 h. The image indicates the presence of supported rhodium clusters along with isolated single Rh atoms. Single Rh atoms are encircled in red. The bright features that are encircled are examples of individual Rh atoms or clusters.

Table 2. Catalytic activities characterizing the sample initially formed by adsorption of $Rh(C_2H_4)_2(acac)$ on DAY zeolite after various treatments for hydrogenation and dimerization of ethylene in a flow reactor at 298 K and 1 bar.[a]

Treatment conditions	Rh–Rh coordination number determined by EXAFS data[b]	Ethylene conversion, (%)	Turnover frequency for ethylene conversion, TOF[c] (s^{-1})	Selectivity in ethylene conversion (wt %)				
				Ethane	*n*-butane	*trans*-2-butene	1-butene	*cis*-2-butene
None	0	2.2	0.11	18.5	0.7	50.1	11.8	18.9
H_2 at 373 K for 4 min	0.18	2.2	0.11	35.1	0.8	34.5	13.6	16.0
H_2 at 373 K for 60 min	4.4	4.9	0.25	64.1	3.1	19.9	4.5	8.4

[a]There was no detectable reaction in the absence of catalyst under our conditions, and the supports alone were catalytically inactive. [b]For the complete set of parameters determined in the EXAFS data fitting, see Table 1. As shown in Table 1, the Rh–Rh coordination number characterizing the untreated sample and that after H_2 treatment at 373 K for 4 min were determined in this work; for comparison, the previously reported Rh–Rh coordination number[36] characterizing the sample after treatment in H_2 at 373 K for 60 min is also shown. [c]Turnover frequency determined from C_2H_4 conversions <5%; catalyst mass = 30 mg; feed partial pressure = 200 mbar C_2H_4, 50 mbar H_2 and 750 mbar He; total flow rate = 100 mL (NTP)/min.

The catalytic behavior of each of the variously treated samples was evaluated for the conversion of ethylene in the presence of H_2 in a once-through isothermal plug-flow reactor at 298 K and 1 bar. The catalyst initially incorporating $Rh(C_2H_4)_2$ supported on the zeolite was active and highly selective for ethylene dimerization (Table 2); ethylene hydrogenation was only a minor side reaction, consistent with earlier observations.[34,39] Our results show that, after contact with a mixture of 50% H_2 in helium at 373 K for 4 min, the TOF characterizing the initial sample incorporating rhodium diethylene complexes was essentially unchanged, but the selectivity for hydrogenation approximately doubled. We infer that replacement of ethylene ligands with hydride and/or formation of small amounts of rhodium pair sites contributed to this change in selectivity. When the initial sample was further treated in a mixture of 50% H_2 in helium at 373 K for 1 h, rhodium clusters (along with some unconverted single-atom rhodium sites) formed, with an average diameter of 0.55 ± 0.10 nm, and, as a result, the catalytic activity increased markedly, and hydrogenation became the dominant reaction (Table 2). This change is as expected, because neighboring rhodium centers favor H_2 dissociation and catalytic hydrogenation of ethylene.[34]

Thus, our data allow a quantification of the changes in the catalyst behavior at the earliest stages of rhodium cluster formation under the influence of H_2. The data show that the rhodium clusters are more highly active catalysts for hydrogenation than the single-site complexes, which are more active for dimerization, consistent with earlier observations.[34]

A bifunctional mechanism has been proposed to explain the dimerization reaction catalyzed by HY zeolite-supported rhodium complexes, occurring as the acidic OH groups on the zeolite surface work in concert with the rhodium complexes.[35,39] In contrast, the hydrogenation reaction

was inferred to involve only the rhodium complexes, proceeding through intermediate ethyl ligands on the rhodium.[39] Earlier work led to the inference[39] of a key role of H_2 activation in the catalysis on the zeolite-supported rhodium species. A slow activation of H_2 on the supported single rhodium complexes boosts the selectivity for dimerization by facilitating the desorption of the product, whereas a fast activation of H_2, as observed on supported rhodium clusters, was inferred to favor the competitive hydrogenation and inhibit the dimerization.[39]

In summary, we monitored the initial steps in the chemistry of H_2-induced cluster formation from supported rhodium complexes by combining IR and EXAFS spectra with STEM images. The activation of H_2 on supported rhodium complexes to form supported rhodium hydride trigged the formation of rhodium clusters (as had been inferred earlier[40]), and our data provide the first evidence of the smallest clusters formed in the process (Rh_2) and their further conversion into higher-nuclearity clusters. These result provide the first evidence showing how the metal nuclearity and ligand environment at the first stages of metal cluster formation influence catalytic activity and selectivity.

EXPERIMENTAL METHODS

Sample synthesis and handling were carried out to minimize exposure to moisture and air. The dealuminated HY zeolite (Zeolite International, CBV760; Si:Al atomic ratio approximately 30) was calcined in O_2 at 773 K for 2 h and evacuated at 773 K for 14 h. $Rh(C_2H_4)_2(acac)$ was chosen as the catalyst precursor. It was brought in contact with the treated zeolite at 298 K in a slurry with *n*-pentane which had been dried and deoxygenated prior to use. After synthesis of the supported catalyst, residual solvent was removed by evacuation. The rhodium content of the resultant powder catalyst was 1.0 wt%.

To form small rhodium clusters, the initially prepared sample was exposed to flowing helium as the temperature was ramped from 298 to 353 K at rate of 3 K/min. Subsequently, the sample was exposed to a mixture of 50% H_2 in helium for 4 min at 1 bar and 373 K, followed by cooling to 298 K and a 60 min soak in helium. To form larger rhodium clusters in the sample, the temperature was increased from 298 to 353 K at rate of 3 K/min with the sample in helium. Then the sample was exposed to 50% H_2 in helium for 60 min at 353 K, followed by cooling to 298 K and a 60 min soak in helium.

STEM samples were prepared by dipping a 200-mesh lacey-carbon-coated copper grid (Ted-Pella) into as-prepared catalyst powders inside an argon-filled glovebox (MBraun, with H_2O and O_2 concentrations <5 ppm). Each sample was transported to the microscope in a sealed stainless-steel Swagelok tube, and the sample was taken out and loaded onto TEM holders in a glovebag (Glas-Col) purged five times with ultra-high-purity argon (Airgas, 99.999%). The holder was then quickly inserted into the microscope, with an estimated exposure time of 2–5 s. To minimize artifacts in the images caused by beam damage, the microscope was aligned for one region of the sample, and then the beam was shifted to a neighboring region for quick image acquisition: 4 μs for a 1024 × 1024 pixel size. This method minimized the exposure of the imaged area to the electron beam.

ASSOCIATED CONTENT

Supporting Information.

Additional information about sample synthesis and handling, IR and EXAFS spectra, and details of the experimental methods. This material is available free of charge via the Internet at http://pubs.acs.org.

AUTHOR INFORMATION

Corresponding Author

*Email: bcgates@ucdavis.edu

Author Contributions

†These authors contributed equally to the paper

Notes

The authors declare no competing financial interests.

ACKNOWLEDGMENTS

This work was supported by the U.S. Department of Energy (DOE), Office of Science, Basic Energy Sciences (BES), Grant DE-FG02-04ER15513. A portion of this work was done as part of the Chemical Imaging Initiative at Pacific Northwest National Laboratory (PNNL) (under Contract DE-AC05-76RL01830), operated for DOE by Battelle. It was conducted under the Laboratory Directed Research and Development Program at PNNL. A portion of the research was performed using EMSL, a national scientific user facility sponsored by the DOE's Office of Biological and Environmental Research and located at PNNL. We acknowledge beam time at beamline 4-1 at the Stanford Synchrotron Radiation Lightsource supported by the DOE Division of Materials Sciences. We thank the beamline staff for valuable support.

REFERENCES

(1) Flytzani-Stephanopoulos, M.; Gates, B. C. Atomically Dispersed Supported Metal Catalysts. *Annu. Rev. Chem. Biomol.* **2012,** *3*, 545-574.
(2) Serna, P.; Gates, B. C. Molecular Metal Catalysts on Supports: Organometallic Chemistry Meets Surface Science. *Acc. Chem. Res.* **2014,** *47*, 2612-2620.
(3) Qiao, B. T.; Wang, A. Q.; Yang, X. F.; Allard, L. F.; Jiang, Z.; Cui, Y. T.; Liu, J. Y.; Li, J.; Zhang, T. Single-Atom Catalysis of CO oxidation using Pt_1/FeO_x. *Nat. Chem.* **2011,** *3*, 634-641.
(4) Guo, X. G.; Fang, G. Z.; Li, G.; Ma, H.; Fan, H. J.; Yu, L.; Ma, C.; Wu, X.; Deng, D. H.; Wei, M. M.; Tan, D. L.; Si, R.; Zhang, S.; Li, J. Q.; Sun, L. T.; Tang, Z. C.; Pan, X. L.; Bao, X. H. Direct, Nonoxidative Conversion of Methane to Ethylene, Aromatics, and Hydrogen. *Science* **2014,** *344*, 616-619.
(5) Yang, M.; Li, S.; Wang, Y.; Herron, J. A.; Xu, Y.; Allard, L. F.; Lee, S.; Huang, J.; Mavrikakis, M.; Flytzani-Stephanopoulos, M. Catalytically Active Au-$O(OH)_x$-species Stabilized by Alkali Ions on Zeolites and Mesoporous Oxides. *Science* **2014,** *346*, 1498-1501.
(6) Gao, J.; Zheng, Y. T.; Jehng, J. M.; Tang, Y. D.; Wachs, I. E.; Podkolzin, S. G. Identification of Molybdenum Oxide Nanostructures on Zeolites for Natural Gas Conversion. *Science* **2015,** *348*, 686-690.
(7) Uzun, A.; Ortalan, V.; Browning, N. D.; Gates, B. C. A Site-isolated Mononuclear Iridium Complex Catalyst Supported on MgO: Characterization by Spectroscopy and Aberration-corrected Scanning Transmission Electron Microscopy. *J. Catal.* **2010,** *269*, 318-328.
(8) Ortalan, V.; Uzun, A.; Gates, B. C.; Browning, N. D. Towards Full-structureDetermination of Bimetallic Nanoparticles with an Aberration-Corrected Electron Microscope. *Nat. Nanotechnol.* **2010,** *5*, 843-847.
(9) Qiao, B. T.; Liang, J. X.; Wang, A. Q.; Xu, C. Q.; Li, J.; Zhang, T.; Liu, J. Y. Ultrastable Single-atom Gold Catalysts with Strong Covalent Metal-Support Interaction (CMSI). *Nano. Res.* **2015,** *8*, 2913-2924.
(10) Yang, M.; Allard, L. F.; Flytzani-Stephanopoulos, M. Atomically Dispersed Au-$(OH)_x$ Species Bound on Titania Catalyze the Low-Temperature Water-Gas Shift Reaction. *J. Am. Chem. Soc.* **2013,** *135*, 3768-3771.
(11) Yang, M.; Liu, J. L.; Lee, S.; Zugic, B.; Huang, J.; Allard, L. F.; Flytzani-Stephanopoulos, M. A Common Single-Site Pt(II)-$O(OH)_x$- Species Stabilized by Sodium on "Active" and "Inert" Supports Catalyzes the Water-Gas Shift Reaction. *J. Am. Chem. Soc.* **2015,** *137*, 3470-3473.
(12) Yang, D.; Xu, P. H.; Guan, E. J.; Browning, N. D.; Gates, B. C. Rhodium Pair-Sites on Magnesium Oxide: Synthesis, Characterization, and Catalysis of Ethylene Hydrogenation. *J. Catal.* **2016,** *338*, 12-20.
(13) Yardimci, D.; Serna, P.; Gates, B. C. Tuning Catalytic Selectivity: Zeolite- and Magnesium Oxide-Supported Molecular Rhodium Catalysts for Hydrogenation of 1,3-Butadiene. *ACS Catal.* **2012,** *2*, 2100-2113.
(14) Yardimci, D.; Serna, P.; Gates, B. C. Surface-Mediated Synthesis of Dimeric Rhodium Catalysts on MgO: Tracking Changes in the Nuclearity and Ligand Environment of the Catalytically Active Sites by X-ray Absorption and Infrared Spectroscopies. *Chem.- Eur. J.* **2013,** *19*, 1235-1245.
(15) Asakura, K.; Kitamurabando, K.; Iwasawa, Y.; Arakawa, H.; Isobe, K. Metal-Assisted Hydroformylation on a SiO_2-Attached Rh Dimer. In Situ EXAFS and FT-IR Observations of the Dynamic Behaviors of the Dimer Site. *J. Am. Chem. Soc.* **1990,** *112*, 9096-9104.

(16) Bando, K. K.; Asakura, K.; Arakawa, H.; Isobe, K.; Iwasawa, Y. Surface Structures and Catalytic Hydroformylation Activities of Rh Dimers Attached on Various Inorganic Oxide Supports. *J. Phys. Chem.* **1996,** *100*, 13636-13645.
(17) Kletnieks, P. W.; Liang, A. J.; Craciun, R.; Ehresmann, J. O.; Marcus, D. M.; Bhirud, V. A.; Klaric, M. M.; Haymann, M. J.; Guenther, D. R.; Bagatchenko, O. P.; Dixon, D. A.; Gates, B. C.; Haw, J. F. Molecular Heterogeneous Catalysis: A Single-site Zeolite-supported Rhodium Complex for Acetylene Cyclotrimerization. *Chem.-Eur. J.* **2007,** *13*, 7294-7304.
(18) Liang, A. J.; Bhirud, V. A.; Ehresmann, J. O.; Kletnieks, P. W.; Haw, J. F.; Gates, B. C. A Site-Isolated Rhodium-Diethylene Complex Supported on Highly Dealuminated Y Zeolite: Synthesis and Characterization. *J. Phys. Chem. B* **2005,** *109*, 24236-24243.
(19) Liang, A. J.; Craciun, R.; Chen, M. Y.; Kelly, T. G.; Kletnieks, P. W.; Haw, J. F.; Dixon, D. A.; Gates, B. C. Zeolite-Supported Organorhodium Fragments: Essentially Molecular Surface Chemistry Elucidated with Spectroscopy and Theory. *J. Am. Chem. Soc.* **2009,** *131*, 8460-8473.
(20) Matsubu, J. C.; Yang, V. N.; Christopher, P. Isolated Metal Active Site Concentration and Stability Control Catalytic CO_2 Reduction Selectivity. *J. Am. Chem. Soc.* **2015,** *137*, 3076-3084.
(21) Miessner, H. Adsorption of Molecular Nitrogen on Rhodium Supported on Dealuminated Zeolite Y; the Formation of Well-Defined Surface Dinitrogen Complexes. *J. Chem. Soc. Chem. Comm.* **1994,** 927-928.
(22) Wovchko, E. A.; Yates, J. T. Activation of O_2 on a Photochemically Generated Rh^I Site on an Al_2O_3 Surface: Low-Temperature O_2 Dissociation and CO Oxidation. *J. Am. Chem. Soc.* **1998,** *120*, 10523-10527.
(23) Khivantsev, K.; Vityuk, A.; Aleksandrov, H. A.; Vayssilov, G. N.; Alexeev, O. S.; Amiridis, M. D. Effect of Si/Al Ratio and Rh Precursor Used on the Synthesis of HY Zeolite-Supported Rhodium Carbonyl Hydride Complexes. *J. Phys. Chem. C* **2015,** *119*, 17166-17181.
(24) Vityuk, A.; Aleksandrov, H. A.; Vayssilov, G. N.; Ma, S. G.; Alexeev, O. S.; Amiridis, M. D. Effect of Si/Al Ratio on the Nature and Reactivity of HY Zeolite-Supported Rhodium Dicarbonyl Complexes. *J. Phys. Chem. C* **2014,** *118*, 26772-26788.
(25) Vityuk, A. D.; Alexeev, O. S.; Amiridis, M. D. Synthesis and Characterization of HY Zeolite-Supported Rhodium Carbonyl Hydride Complexes. *J. Catal.* **2014,** *311*, 230-243.
(26) Argo, A. M.; Gates, B. C. MgO-Supported Rh_6 and Ir_6: Structural Characterization during the Catalysis of Ethene Hydrogenation. *J. Phys. Chem. B* **2003,** *107*, 5519-5528.
(27) Argo, A. M.; Odzak, J. F.; Goellner, J. F.; Lai, F. S.; Xiao, F. S.; Gates, B. C. Catalysis by Oxide-Supported Clusters of Iridium and Rhodium: Hydrogenation of Ethene, Propene, and Toluene. *J. Phys. Chem. B* **2006,** *110*, 1775-1786.
(28) Graydon, W. F.; Langan, M. D. Rhodium Cluster Ultradispersed Catalysts of High and Low Activity. *J. Catal.* **1981,** *69*, 180-192.
(29) Vidal, J. L.; Walker, W. E. Rhodium-Carbonyl Cluster Chemistry under High-Pressure of Carbon-Monoxide and Hydrogen. 1. Infrared Spectroscopic Study of Homogeneous Systems Active in the Catalytic Synthesis of Polyalcohols from CO and H_2. *Inorg. Chem.* **1980,** *19*, 896-903.
(30) Hoxha, F.; van Vegten, N.; Urakawa, A.; Krurneich, F.; Mallat, T.; Baiker, A. Remarkable Particle Size Effect in Rh-Catalyzed Enantioselective Hydrogenations. *J. Catal.* **2009,** *261*, 224-231.
(31) Ligthart, D. A. J. M.; Van Santen, R. A.; Hensen, E. J. M. Supported Rhodium Oxide Nanoparticles as Highly Active CO Oxidation Catalysts. *Angew. Chem. Int. Edit.* **2011,** *50*, 5306-5310.

(32) McClure, S. M.; Lundwall, M. J.; Goodman, D. W. Planar Oxide Supported Rhodium Nanoparticles as Model Catalysts. *Proc. Natl. Acad .Sci. U.S.A.* **2011,** *108*, 931-936.
(33) Xu, S.; Li, J.; Yang, D.; Hao, J. Promotional Mechanism of Sulfation on Selective Catalytic Reduction of NO by Methane in Excess Oxygen: A Comparative Study of Rh/Al_2O_3 and $Rh/Al_2O_3/SO_4^{2-}$. *J. Phys. Chem. C* **2008,** *112*, 16052-16059.
(34) Serna, P.; Gates, B. C. Zeolite-Supported Rhodium Complexes and Clusters: Switching Catalytic Selectivity by Controlling Structures of Essentially Molecular Species. *J. Am. Chem. Soc.* **2011,** *133*, 4714-4717.
(35) Serna, P.; Gates, B. C. Zeolite- and MgO-supported Rhodium Complexes and Rhodium Clusters: Tuning Catalytic Properties to Control Carbon-carbon vs. Carbon-hydrogen Bond Formation Reactions of Ethene in the Presence of H_2. *J. Catal.* **2013,** *308*, 201-212.
(36) Liang, A. J.; Gates, B. C. Time-Resolved Structural Characterization of Formation and Break-up of Rhodium Clusters Supported in Highly Dealuminated Y Zeolite. *J. Phys. Chem. C* **2008,** *112*, 18039-18049.
(37) Jentys, A. Estimation of Mean Size and Shape of Small Metal Particles by EXAFS. *Phys. Chem. Chem. Phys.* **1999,** *1*, 4059-4063.
(38) Kip, B. J.; Duivenvoorden, F. B. M.; Koningsberger, D. C.; Prins, R. Determination of Metal-Particle Size of Highly Dispersed Rh, Ir, and Pt Catalysts by Hydrogen Chemisorption and EXAFS. *J. Catal.* **1987,** *105*, 26-38.
(39) Serna, P.; Gates, B. C. A Bifunctional Mechanism for Ethene Dimerization: Catalysis by Rhodium Complexes on Zeolite HY in the Absence of Halides. *Angew. Chem. Int. Edit.* **2011,** *50*, 5528-5531.
(40) Serna, P.; Yardimci, D.; Kistler, J. D.; Gates, B. C. Formation of Supported Rhodium Clusters from Mononuclear Rhodium Complexes Controlled by the Support and Ligands on Rhodium. *Phys. Chem. Chem. Phys.* **2014,** *16*, 1262-1270.